The role of nonlinear effects in the propagation of noise from high-power jet aircraft[a)]

Kent L. Gee[b)] and Victor W. Sparrow
Graduate Program in Acoustics, 201 Applied Science Building, The Pennsylvania State University, University Park, Pennsylvania 16802

Michael M. James,[c)] J. Micah Downing,[c)] and Christopher M. Hobbs
Wyle Laboratories, 241 18th Street South, Suite 701, Arlington, Virginia 22202

Thomas B. Gabrielson and Anthony A. Atchley
Graduate Program in Acoustics, 201 Applied Science Building, The Pennsylvania State University, University Park, Pennsylvania 16802

(Received 29 September 2007; revised 7 March 2008; accepted 10 March 2008)

To address the question of the role of nonlinear effects in the propagation of noise radiated by high-power jet aircraft, extensive measurements were made of the F-22A Raptor during static engine run-ups. Data were acquired at low-, intermediate-, and high-thrust engine settings with microphones located 23–305 m from the aircraft along several angles. Comparisons between the results of a generalized-Burgers-equation-based nonlinear propagation model and the measurements yield favorable agreement, whereas application of a linear propagation model results in spectral predictions that are much too low at high frequencies. The results and analysis show that significant nonlinear propagation effects occur for even intermediate-thrust engine conditions and at angles well away from the peak radiation angle. This suggests that these effects are likely to be common in the propagation of noise radiated by high-power aircraft. © *2008 Acoustical Society of America.* [DOI: 10.1121/1.2903871]

PACS number(s): 43.25.Cb, 43.50.Nm, 43.25.Vt [ROC] Pages: 4082–4093

I. INTRODUCTION

The role of nonlinearity in the propagation of noise radiated from high-speed jets is a question that has been the topic of investigations that span the last few decades. From the perspective of investigations on full-scale jets, Morfey and Howell[1] showed that flyover measurements made on the Concorde and other high-power aircraft exhibited anomalously low atmospheric absorption at high frequencies; an analysis of their recording equipment and the measurement environment indicated that nonlinear energy transfer to high frequencies was a possible explanation for the anomalously low absorption. More recently, analyses by Gee *et al.*[2,3] of the F/A-18E Super Hornet engine run-up data have shown evidence of nonlinear energy transfer in terms of measured versus linearly predicted spectra at multiple distances, as well as by calculations of nonlinearity indicators. Model-scale jet noise experiments that demonstrate evidence of nonlinear propagation effects include those by Gallagher and McLaughlin,[4] Petitjean *et al.*,[5] and Gee *et al.*[6]

Others have been motivated by the hypothesis that nonlinear effects are present in high-amplitude jet noise but have approached the problem indirectly by conducting controlled-source measurements or by performing numerical experiments. Pernet and Payne[7] studied the nonlinear evolution of noise signals in a plane-wave tube. Pestorius and Blackstock[8] extended the scope of Pernet and Payne's original work by propagating noise of greater bandwidth and amplitude in their duct. They also developed a nonlinear propagation algorithm that Pierce[9] later showed to be a numerical solution to the generalized Burgers equation (GBE). Blackstock[10] later used a modified version of their code to numerically propagate a noise recording from a T-38 aircraft at close range. The code predicted a nonlinear evolution of the waveform, but no measurements of the aircraft noise at greater distances were available for comparison against the prediction. Additionally, Webster and Blackstock[11] carried out free-field, high-amplitude noise experiments with an array of horn-coupled loudspeakers. They found significant evidence of nonlinear energy transfer in many of their experiments. Furthermore, when their controlled-source noise spectra were compared to a measured spectrum from a KC-135A aircraft, the controlled-source spectral levels were found to be considerably lower, suggesting that nonlinearity likely affected noise propagation from the KC-135A and other high-power aircraft. Similar arguments were made by Gee *et al.*[12] in the conclusions of a recent propagation study that employed a large horn-coupled electropneumatic driver as a source. Finally, Crighton and Bashforth,[13] Scott,[14] Lighthill,[15] Punekar,[16] and Menounou and Blackstock[17] have all analytically or numerically looked at aspects of the nonlinear propagation of noise.

[a)]Portions of this work were presented at the 2005 Joint Acoustical Society of America and Noise-Con Meeting in Minneapolis, MN and at the 12th AIAA/CEAS Aerocoustics Conference in Monterey, CA, May 2006.

[b)]Present address: Department of Physics and Astronomy, N243 ESC, Provo, UT 84602; electronic mail: kentgee@byu.edu

[c)]Present address: Blue Ridge Research and Consulting, LLC, 13 $\frac{1}{2}$ W. Walnut St., Asheville, NC 28801.

 © 2008 Acoustical Society of America

Redistribution subject to ASA license or copyright; see http://acousticalsociety.org/content/terms. Download to IP: 128.187.97.22 On: Mon, 17 Mar 2014 20:38:46

A broad look at these prior studies tells us that there is certainly compelling evidence that nonlinear effects can influence the propagation of high-amplitude jet noise. However, despite these numerous previous investigations, there has not yet been an experiment that comprehensively addresses, from experimental and modeling standpoints, the question of the prevalence or significance of nonlinear effects in the propagation of noise radiated from a full-scale, high-power (e.g., military) jet aircraft.

In this article, we demonstrate that the propagation of noise from a high-power military jet aircraft can be highly nonlinear. We present the outcome of propagation measurements made on an F-22A Raptor during static engine run-up tests and compare the measured spectra against those predicted by two propagation models. The first model is a GBE-based nonlinear model[18] that is related to the work of Anderson[19] and Pestorius and Blackstock.[8] This model has been recently used to study the outdoor propagation of finite-amplitude periodic signals.[12] The second model is a free-field, linear propagation model that includes the effects of spherical spreading and atmospheric absorption and dispersion. The comparisons show that nonlinear effects are significant for multiple angles and engine powers and are not limited to, for example, the Mach wave (peak radiation) angle at afterburner. The scope of this article is significantly broader than that of Refs. 20 and 21, in which preliminary results were presented.

II. OVERVIEW OF PROPAGATION MODELS

A. Nonlinear model

The nonlinear propagation model is based on a formulation of the GBE that incorporates cumulative quadratic nonlinearity, atmospheric absorption and dispersion, and spherical spreading. In a retarded time frame, this formulation of the GBE may be written as

$$\frac{\partial p}{\partial r} = \frac{\beta}{2\rho_0 c_0^3}\frac{\partial p^2}{\partial \tau} + \psi_\tau\{p\} - \frac{1}{r}p, \tag{1}$$

where $p(r,\tau)$ is the acoustic pressure, r is the range variable, τ is the retarded time of propagation between the input distance and r, β is the coefficient of nonlinearity, ρ_0 is the ambient atmospheric density, c_0 is the small-signal sound speed, and ψ_τ is an operator representing atmospheric absorption and dispersion that acts on $p(r,\tau)$.

Equation (1) is solved with a hybrid time-frequency domain algorithm that is based on the work of Anderson[19] and Pestorius and Blackstock[8] and is described in detail in Ref. 18. Briefly, in the hybrid time-frequency domain solution of the GBE, an input time waveform is propagated to a greater distance via small spatial steps (in our case, one-tenth of the shock formation distance at each propagation step). Because the GBE formulation in Eq. (1) shows that the evolution of the pressure with distance is equal to the addition of three separate terms for a sufficiently small spatial step, the nonlinear and linear portions of the propagation can be treated independently over this spatial step. This allows the nonlinearity to be accounted for with the implicit Earnshaw solution in the time domain, whereas the absorption and dispersion are most conveniently handled in the frequency domain on a frequency-by-frequency basis. The spherical spreading term is a simple scaling factor in either domain but is evaluated in the frequency domain in our algorithm. A fast Fourier transform (FFT) and its inverse are used to transform the waveform to the frequency domain and back at each spatial step. Finally, in applying atmospheric absorption and dispersion to the complex pressure spectrum in the frequency domain, we are performing a FFT-based circular convolution. Because of the relatively rapid decay of the corresponding impulse response of the complex absorption transfer function, wraparound artifacts were effectively suppressed with a cosine-squared amplitude taper to the first and last 100 samples of the time waveform.

B. Linear model

It is the first term in Eq. (1) involving $\partial p^2/\partial\tau$ that produces nonlinearity; without it, Eq. (1) is simply a free-field parabolic propagation model that contains spherical spreading and atmospheric absorption and dispersion. This linearized form of Eq. (1) is the prediction model used in this study for comparisons of linear propagation versus the experiment. To obtain linearly predicted waveforms, the input waveforms are transformed to the frequency domain, where the spherical spreading and atmospheric absorption and dispersion over the propagation distances are applied. The complex pressure spectra are then inverse Fourier transformed back to the time domain to obtain the linearly predicted waveform at the comparison distance. Although this process is similar to the nonlinear model, the linear nature of these calculations allows each propagation prediction to be performed in a single spatial step.

III. MEASUREMENT SUMMARY

A. Experimental setup

Static engine run-up tests were conducted by Wyle Laboratories and Penn State for the F-22A Raptor during the early morning on 15 September 2004 at Edwards Air Force Base (EAFB). The F-22A Raptor has two Pratt and Whitney F-119 turbofan engines that are in the 160 kN (35 000 lbf) thrust class and have two-dimensional convergent-divergent nozzles capable of $\pm 20\,^\circ$ thrust vectoring. (Additional information regarding the engine operating parameters is not publicly available at this time.) To measure the acoustical radiation from an engine, Bruel and Kjaer (types 4938, 4939, and 4190) and GRAS (type 40BF) condenser microphones were located at various distances along five different radials, all at a height of approximately 1.8 m. The microphone layout is shown in Fig. 1, where angles are measured relative to the jet inlet. The origin for the measurement array was located approximately 5.5 m (roughly seven to eight jet diameters) downstream from the jet nozzles. This origin reflected an attempt to locate the origin as close as possible to the dominant aeroacoustic source region downstream of the nozzle exit plane. This location, however, is only an approximation at best because not only are the exact source characteristics currently unknown, but the dominant source region is expected to vary both as a function of frequency and angle.

Redistribution subject to ASA license or copyright; see http://acousticalsociety.org/content/terms. Download to IP: 128.187.97.22 On: Mon, 17 Mar 2014 20:38:46

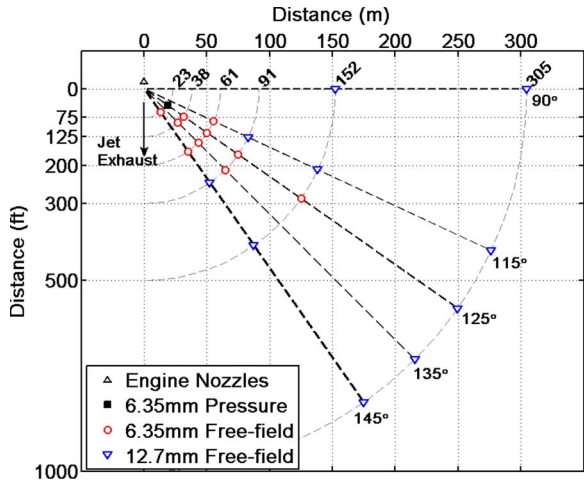

FIG. 1. (Color online) Experimental setup for the F-22A measurements at Edwards Air Force Base. Distances are shown in meters along the horizontal axis and in feet along the vertical axis.

During the tests, the engine farthest from the measurement array was held idle while the near engine's condition was varied for the run-up tests.

With the exception of the 23 m, 125° microphone, which was a 4938 pressure sensor, all microphones were free-field sensors. The 4938, 4939, and 40BF microphones have a 6.35 mm (0.25 in.) diameter diaphragm, whereas the 4190 microphones have a 12.7 mm (0.5 in.) diameter diaphragm. The 4190 microphones were located along 90° and along the 305 m arc. Because of limitations in setup time caused by security restrictions, all microphones were mounted vertically at grazing incidence, which is a nonideal configuration for the free-field sensors and affects their high-frequency response. Acquisition of the pressure waveforms was carried out using National Instruments 24 bit PXI-4472 DAQ cards with a 96 kHz sampling rate.

B. Local meteorology

The time of the tests was selected to be early morning in the hope of minimizing atmospheric effects that are usually present during the day at EAFB, namely, a significant temperature lapse and moderate winds. The run-up measurements took place between 6:30 and 8:00 a.m. Pacific daylight time (PDT), during which time atmospheric conditions were generally conducive to making propagation measurements. A meteorological station, placed at 61 m and 122.5°, monitored the local conditions during the test. The station consisted of three temperature sensors located at heights of 0.3, 1.7, and 3.3 m, two relative humidity sensors located at 0.3 and 3.3 m, and wind speed and direction gauges located at 4.3 m. Plots of the meteorological conditions during the entire testing period may be found in Ref. 18. The results of the monitoring show that relatively neutral measurement conditions occurred toward the end of the test, at approximately 7:30 a.m., when there was low wind (<0.5 m/s) and little temperature gradient (<0.3 °C/m) at the station. The particular measurements discussed hereafter were taken between 7:35 and 7:50 a.m., during which this favorable measurement environment appeared to persist. Shown in Table I are the average conditions during the three particular runs discussed in this article, which represent low engine power (idle), intermediate engine power (90% rpm), and high engine power (afterburner).

C. Expected influence of ground reflections

The jet source and microphones are both located off the ground; consequently, multipath interference effects caused by ground reflections are expected to be present in the spectra. Because both the nonlinear and linear propagation models described in Sec. II are free-field models that do not incorporate ground reflections, it is important to understand at the outset the expected effect of ground reflections on spectral behavior. A characterization of ground-induced interference effects explains the presence of "ripples" in the one-third octave spectra calculated from the measured waveforms. In addition, it illustrates that the effect of the ground cannot explain the large discrepancy that will be shown between measured spectra and predicted spectra based on the free-field linear model described in Sec. II B.

The measurements were conducted on a runway located in a dry lake bed that was several hundred meters from any buildings or other large obstructions. The terrain was extremely flat; however, the composition of the terrain varied over the measurement area, beginning with a tarmac that gave way to a lake bed loosely covered with sage brush and followed by a bare lake bed. The difference in surface hardness between the tarmac and the lake bed constitutes an impedance change along the propagation path for which an explicit accounting would normally be required. However, because the ground impedances for the various surface compositions were not measured and because lookup tables of the effective flow resistivity for various types of ground (e.g., see Ref. 22) give a rather wide range for each surface, accounting for an impedance change is not likely to be very helpful. Rather, a constant ground impedance that falls

TABLE I. Measurement times and mean ambient conditions for the F-22A engine run-up test. The temperature and relative humidity conditions have been estimated at 1.8 m via linear interpolation between measurement heights. Temperatures have been rounded to the nearest half-degree and relative humidity values to the nearest percent. Wind speeds given are at the measured height of 4.3 m.

Engine condition	Time (PDT)	Pressure (atm)	Temperature (°C)	Relative hum. (%)	Mean wind speed (m/s)
Idle	7:35	0.92	15.0	48	0.1
90% rpm	7:49	0.92	16.5	51	0.5
Afterburner	7:36	0.92	15.0	48	0.1

Redistribution subject to ASA license or copyright; see http://acousticalsociety.org/content/terms. Download to IP: 128.187.97.22 On: Mon, 17 Mar 2014 20:38:46

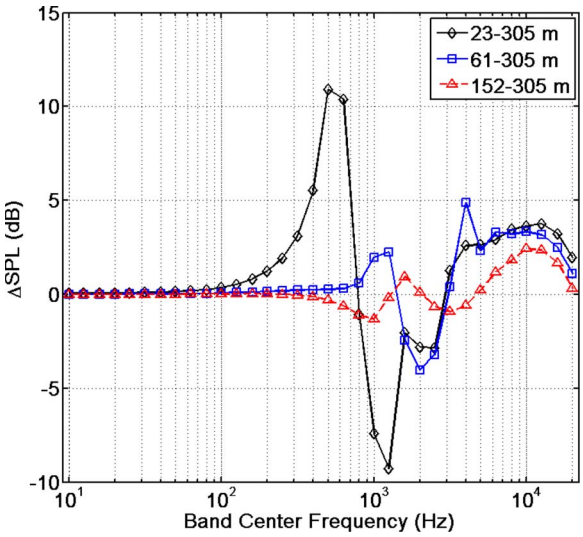

FIG. 2. (Color online) Predicted change in sound pressure level (relative to free-field predicted levels) due to ground interactions (ΔSPL) between 1.8 m high microphones for various ranges as a function of one-third octave band center frequency.

within the range of "hard ground" has been used in calculations with the recognition that the analysis is a somewhat qualitative assessment of the anticipated impact of the ground on spectral calculations.

The particular model used to make these ground reflection calculations accounts for the interaction of spherically spreading waves with a finite-impedance ground[23] as well as the effects of turbulence[24] on spectral minima and maxima. In these calculations, the point source and the receiver are both assumed to be located at a height of 1.8 m. An effective flow resistivity of 4000 kPa s/m^2 has been assumed, which nominally corresponds to exposed, rain-packed dirt.[22] The turbulence model[24] employed has as input parameters a turbulence length scale and a fluctuating index of refraction, which were set to 1.1 m and 3.0×10^{-6}, respectively.

The relative change in the free-field sound pressure level due to the ground, ΔSPL, is shown in Fig. 2 as a function of one-third octave band center frequency for the propagation ranges used subsequently in the prediction model comparisons. Calculations of ΔSPL between two measurement distances, rather than simply at a single distance, is appropriate for the current scenario because the waveform data at the model input distance also contain the effects of ground reflections. Consequently, Fig. 2 describes the differences in interference effects for the two measurement distances. The ΔSPL values for 23–305, 61–305, and 152–305 m shown in Fig. 2 demonstrate that the dominant ground interactions occur between 500 Hz and 5 kHz for these propagation ranges. It is important to note that at higher frequencies, the influence of the ground is only approximately a 2–3 dB increase in sound pressure level relative to a linear, free-field prediction made between the two microphone locations.

Before proceeding to an analysis of the measurement results in Sec. IV, it is noted that ground effects will be readily apparent in the one-third octave spectra calculated from the measured time data. However, the spectral nulls are not as deep and are significantly broader, particularly for the 90% rpm and afterburner cases, than indicated by this theoretical analysis. This may be attributed to the partially correlated nature and the spatial extent of the aeroacoustic sources in the jet plume, as opposed to the point source assumed in the ground reflection model. In addition, the frequencies at which the nulls occur also differ somewhat from the analysis, particularly for 91–305 m, which is certainly caused at least in part by the estimated values of the flow resistivity and turbulence coefficients. These discrepancies serve to make quantitative application of the theory in the form of spectral corrections inappropriate. However, the analysis is qualitatively useful in that (a) ground reflections may be identified as such in the measured spectra and that (b) the effect of the ground cannot reasonably explain the difference between measured spectra and spectra predicted using free-field, linear theory.

IV. MEASUREMENT RESULTS

In this section, one-third octave spectra calculated from the measured waveforms (hereafter referred to as measured one-third octave spectra) are shown as a function of distance for various engine powers and as a function of angle at two distances for one engine at afterburner. To calculate the spectrum, a waveform consisting of 2^{20} samples (about 10.9 s) was filtered with one-third octave filters to yield the average power in each band. The band pressure levels were then calculated from the average powers. To account for the placement of the free-field microphones at grazing incidence, manufacturer-supplied corrections have been added to the calculated spectra. For the 4190 microphones, the correction at 10 kHz is approximately 4 dB and grows to about 10 dB at 20 kHz. If these corrections are applied to one-third octave spectra, the maximum uncertainty of the correction is 2 dB for cases where the power in the 20 kHz one-third octave band is concentrated at either edge of the band. For the 4939 and 40BF microphones, the correction is relatively minor, only 2.5 dB at 20 kHz, with an uncertainty of less than 1 dB. Also presented in this section are time waveform segments for the near engine at 90% rpm and afterburner.

A. Function of engine power

1. Idle

The measured one-third octave spectra along 125° for idle, which represents the low-power case, are displayed in Fig. 3. The frequency axis has been restricted, from the 20 Hz to 4 kHz one-third octave bands, because instrumentation noise floor limits were reached outside this range at some of the distances. Because the jet mixing noise is relatively low in amplitude, the spectral shape at idle is not a characteristic "haystack" shape common in jet noise but contains other components of the overall engine noise. Further examination of the measured spectra between 23 and 305 m shows the effects of geometrical spreading and a gradual roll-off at high frequencies caused by atmospheric absorption. Also present is the influence of ground reflections, most noticeable for 23–61 m and above about 500 Hz. Finally, in the legend of Fig. 3, as well as those of subsequent figures, the overall sound pressure level (traditionally abbreviated as

Redistribution subject to ASA license or copyright; see http://acousticalsociety.org/content/terms. Download to IP: 128.187.97.22 On: Mon, 17 Mar 2014 20:38:46

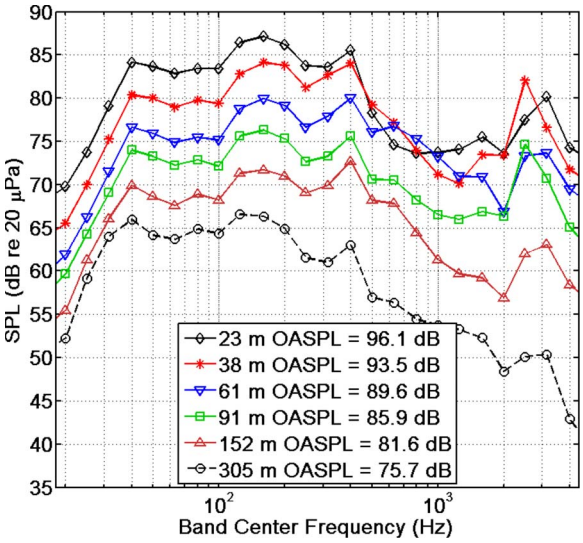

FIG. 3. (Color online) Measured one-third octave levels along 125° for idle. The measurement system noise floor limits the analysis range to the 20 Hz–4 kHz one-third octave bands. In this and in subsequent figure legends, OASPL refers to the overall sound pressure level.

OASPL within the aeroacoustics community) is given. Here, the OASPL values indicate levels that, from an occupational noise perspective, would be potentially damaging at close range if hearing protection is not worn but not high enough that nonlinear propagation effects would likely be significant.

2. 90% rpm

With the engine nearest to the measurement array at 90% rpm, the jet mixing noise is sufficient in amplitude to cause the spectra along 125° to have the characteristic haystack shape expected of jet noise close to the source. On a narrowband scale, the 23 m spectrum in Fig. 4(a) would exhibit a frequency-squared dependence at low frequencies (6 dB/octave increase) and an inverse-frequency-squared dependence at high frequencies (6 dB/octave decrease). However, because of the rate of increase of the one-third octave bandwidths, one-third octave spectra exhibit a frequency-cubed dependence at low frequencies (9 dB/octave increase) and an inverse-frequency dependence at high frequencies (3 dB/octave decrease). With the exception of the ground effects between 500 and 3 kHz, the high-frequency roll-off at 23 m obeys the expected 3 dB/octave trend. Furthermore, it is noteworthy that the slope of the roll-off does not appear to significantly change between 23 and 91 m, which could indicate nonlinear waveform steepening and shock formation during the course of propagation.

Some further discussion regarding evidence of nonlinear propagation is worthwhile at this stage. The OASPL values for 90% rpm are substantially greater than for idle and are large enough that nonlinear effects may be expected when compared to the results of past experiments with controlled sources.[11,12] The evolution of the high-frequency roll-off between 23 and 305 m in Fig. 4(a) suggests that these nonlinear effects are indeed present. According to nonlinear theory,[25] significant shock formation in a random noise waveform will cause the high-frequency spectrum to exhibit a 6 dB/octave roll-off (3 dB/octave on a one-third octave scale). This power-law roll-off will continue out to a frequency that is on the order of the characteristic inverse shock rise time, where it is replaced with an exponential roll-off. As the waveform travels farther, atmospheric absorption causes the shocks to begin to unsteepen and the frequency at which the power law gives way to the exponential roll-off to decrease. Examination of the high-frequency spectral trends in Fig. 4(a) shows that they appear to mimic this behavior. Between 23 and 91 m, little change occurs in the spectral slope out to 20 kHz, suggesting that significant shocks have formed. By 152 m, the power-law roll-off has given way to an exponential roll-off above 5 kHz and the frequency at which this transition occurs decreases by 305 m.

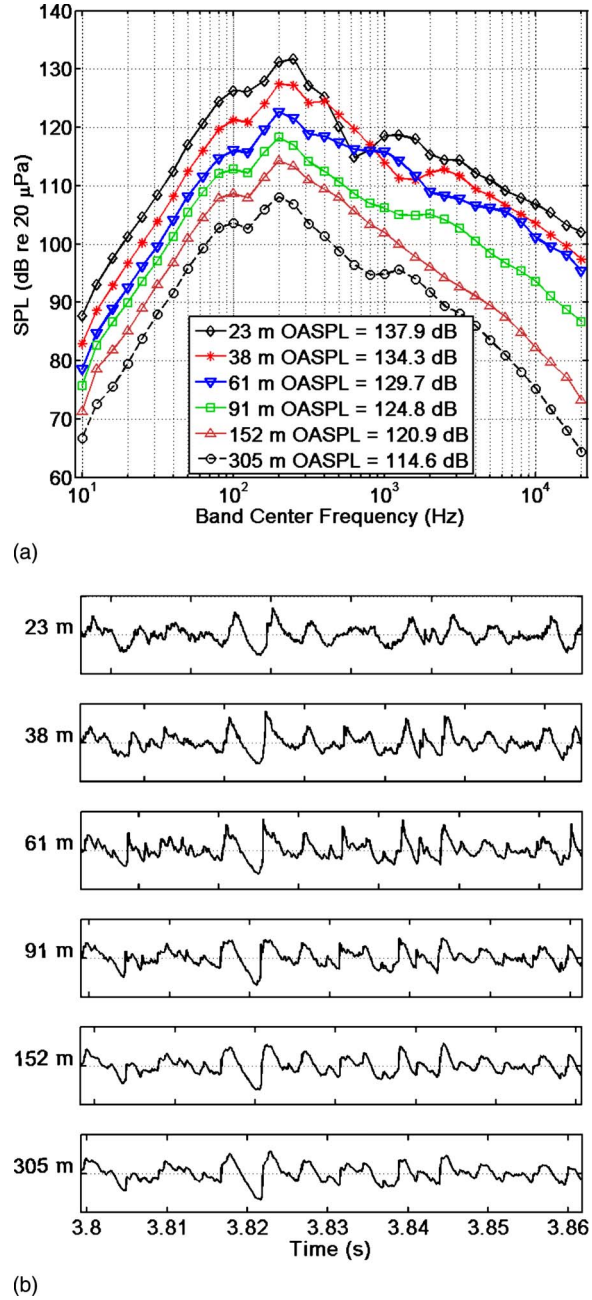

FIG. 4. (Color online) (a) Measured one-third octave levels along 125° for one engine at 90% rpm. (b) Amplitude-scaled and time-aligned waveform segments at 23–305 m. The ordinate limits for each waveform are ±800 Pa.

Redistribution subject to ASA license or copyright; see http://acousticalsociety.org/content/terms. Download to IP: 128.187.97.22 On: Mon, 17 Mar 2014 20:38:46

Additional evidence of this phenomenon can be seen by examining a small segment of the 90% rpm time waveform at each of the distances. Time-aligned portions of the waveforms that have been amplitude scaled by multiplying them by the ratio of the measurement distance and 23 m, which removes the effects of assumed spherical spreading, are displayed in Fig. 4(b). Visual analysis of the time waveform suggests a steepening trend that continues out to 61 or 91 m. Beyond 91 m, some of the shocks that have formed appear to thicken, which suggests the increasing relevance of atmospheric losses that manifest themselves as the exponential roll-off in the spectra in Fig. 4(a).

3. Afterburner

The measurement results for afterburner and 125°, displayed in Fig. 5, are similar to those of 90% rpm and so only significant differences are mentioned. First, Fig. 5(a) shows that, relative to 90% rpm, OASPL values have increased by 5–7 dB at each of the measurement locations. This suggests a greater importance of nonlinear effects, which is corroborated by the fact that the high-frequency spectral decay rate in Fig. 5(a), although somewhat complicated by the ground reflections, is clearly less than that for 90% rpm at 152 and 305 m. A qualitative comparison of the afterburner waveform segments (again amplitude scaled to remove spherical spreading) in Fig. 5(b) with the 90% rpm waveforms in Fig. 4(b) reveals that the shocks present in the afterburner waveform at 305 m appear to have shorter rise times than those in the 90% rpm waveform. The shock rise time comparison agrees with the observed high-frequency behavior in the spectra for the two engine conditions.

B. Function of angle

The microphone layout for the propagation experiments, displayed in Fig. 1, showed that four 6.35 mm microphones were located between 115° and 145° at 61 m. The measured one-third octave spectra for these microphones and the near engine at afterburner are displayed in Fig. 6(a). The spectra are similar at the four angles, with similar OASPL values, although the spectral peak frequency and the severity of the ground interference nulls both vary as a function of angle.

At 305 m, in addition to 115°–145°, a microphone was also located at 90°. The 305 m, afterburner spectra for these angles is shown in Fig. 6(b). Because the primary radiation direction of the jet mixing noise is to the rear of the aircraft, the peak-frequency region of the spectrum at 90° is somewhat ill defined and the OASPL is 10–12 dB less than the other angles. Given the lower OASPL at this angle, nonlinear effects would likely play a lesser role, so it is not surprising that the rate of the high-frequency roll-off is much greater at 90° than at the other angles. This is not to say that nonlinear effects do not play some role at 90°, however. Comparisons between measurement and predicted spectra along 90° and other angles are shown in Sec. V to determine the level of agreement between models and experiment as well as the relative significance of nonlinear propagation effects for a given case.

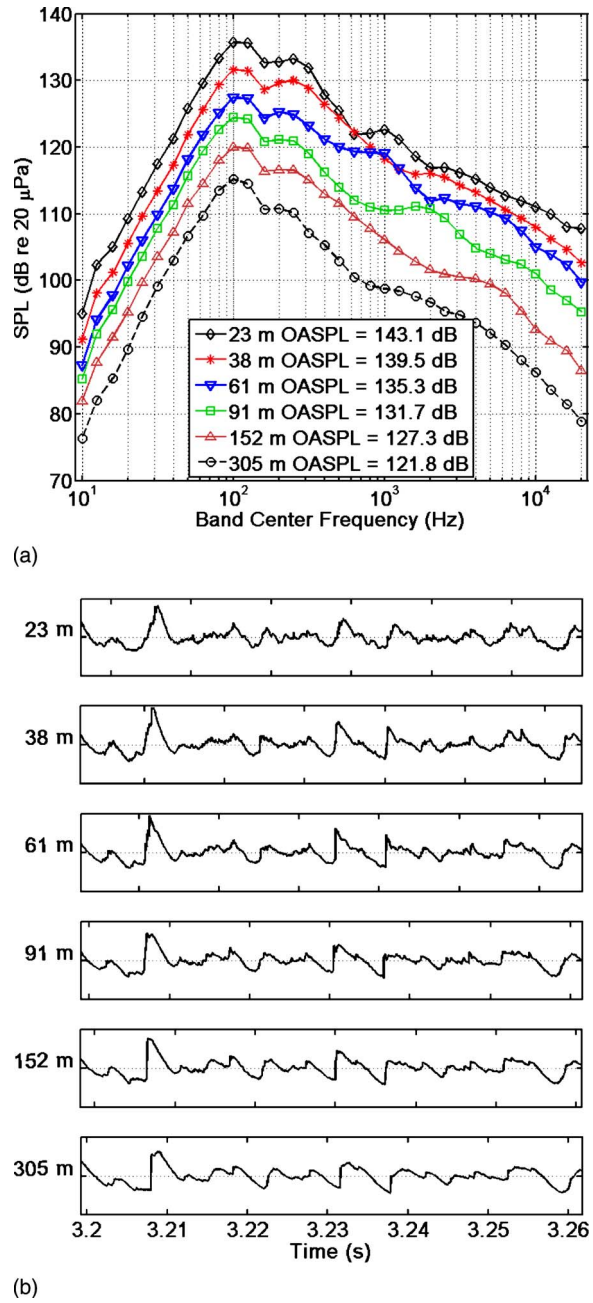

FIG. 5. (Color online) (a) Measured one-third octave levels along 125° for one engine at afterburner. (b) Amplitude-scaled and time-aligned waveform segments at 23–305 m. The ordinate limits for each waveform are ±1800 Pa.

V. COMPARISONS WITH MODELS

This section contains several comparisons between measured spectra and spectra predicted from free-field linear and nonlinear GBE-based propagation models. The comparisons are divided into three sections: (a) comparisons as a function of engine power (idle, 90% rpm, and afterburner) along 125°, (b) GBE model comparisons as a function of algorithm input distance, and (c) comparisons as a function of propagation angle for both 90% rpm and afterburner. It is noted at the outset that these comparisons are largely visual, with mention of the level of agreement at specific frequencies made. A prior study,[12] in which similar model-versus-measurement comparisons were made using a high-

Redistribution subject to ASA license or copyright; see http://acousticalsociety.org/content/terms. Download to IP: 128.187.97.22 On: Mon, 17 Mar 2014 20:38:46

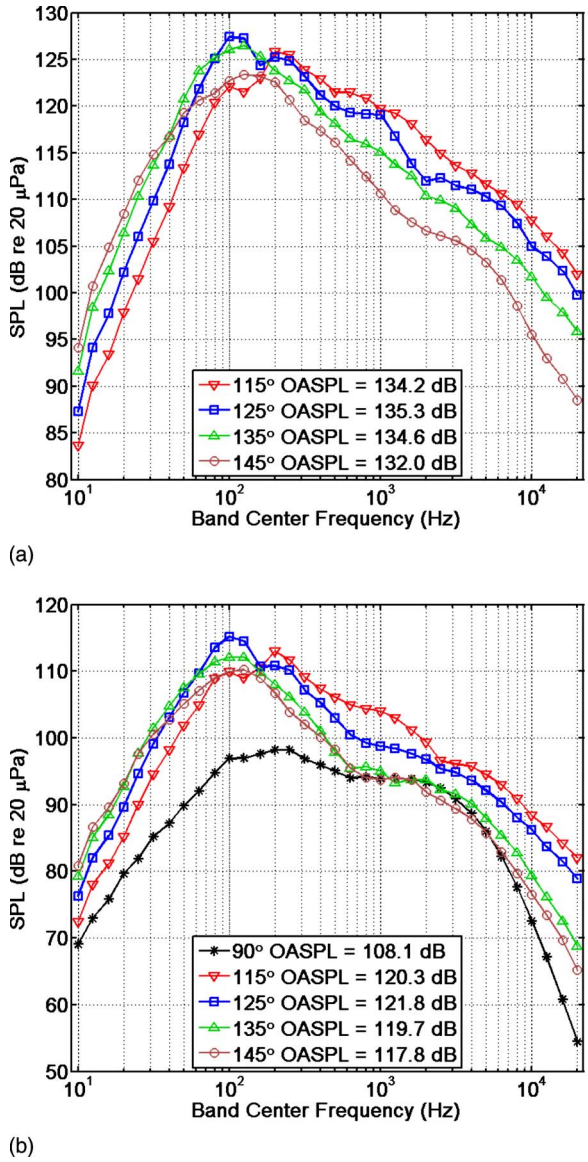

FIG. 6. (Color online) Measured afterburner one-third octave levels at (a) 61 m and (b) 305 m.

amplitude controlled source, employed a quantity called the mean absolute error to quantify differences between measurement and predictions. However, the significance of this quantity is somewhat artificial in the sense that the greatest contributions to the mean absolute error for the case of significant nonlinearity and even moderate propagation ranges will come at the highest frequencies analyzed, where the difference between a linear prediction and the measurement will be the greatest. Because of the drastically different functional forms of the high-frequency spectral behavior for the linearly predicted and the measured spectra, use of the mean absolute error has been discarded in this article, leaving the comparisons between model and experiment mainly visual in nature.

As described in Sec. II, nonlinearly and linearly predicted waveforms were obtained by evaluating the nonlinear and linear[26] models out to the propagation comparison distance, which is 305 m. The input waveforms consisted of approximately 10.9 s of data (2^{20} samples), the same waveform length used to obtain the one-third octave spectra in Figs. 3, 4(a), and 5(a). To provide the most consistent comparison between models and experiment, the input waveforms used were time aligned via the retarded time to account for the propagation delay between input and receiver distances. Once the linearly and nonlinearly predicted waveforms were obtained, the predicted one-third octave spectra were calculated with the same one-third octave filtering procedure used to process the experimental data.

A. Function of engine power

The first set of comparisons carried out is for the three different engine powers with the propagation range and angle held constant. For ease of discussion, the low and high engine power results are presented first, followed by the results from the intermediate engine setting.

1. Idle

The measured and predicted spectra for both engines at idle and 125° are displayed in Fig. 7. The agreement between the 23–305 m predictions and the 305 m measurement is not extremely good; a free-field, homogeneous atmosphere model does not match the measurement with great success. Based on a study of all the data sets acquired between 6:30 and 8:00 a.m., we believe that the cause of the disagreement between the models and the measurement at low frequencies (<200 Hz) is meteorological in nature because it is not always present in the data sets (e.g., the 90% rpm test to be shown subsequently). In contrast, the disagreement between 500 Hz and 2 kHz is principally caused by ground reflections. The near equivalence of the two predicted spectra is significant and indicates that the GBE-based model predicts negligible nonlinear effects, at least out to the maximum comparison range of 4 kHz. Finally, of particular importance to subsequent comparisons between engine conditions is the fact that above 2 kHz, the measurement and models agree to within 1 dB.

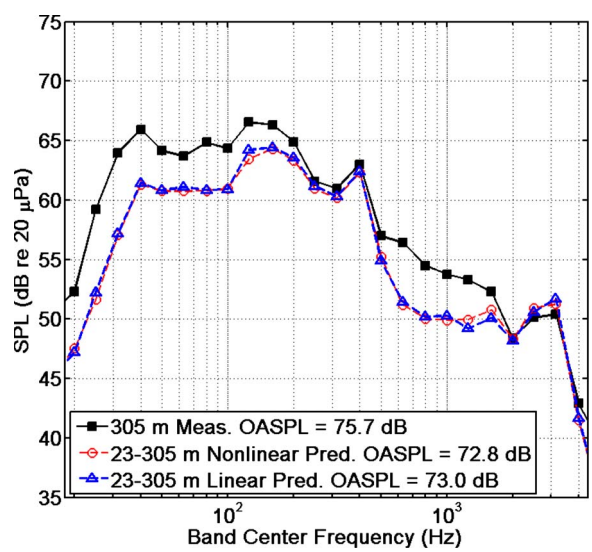

FIG. 7. (Color online) Comparison between predicted spectra and measurement for idle along 125°.

Redistribution subject to ASA license or copyright; see http://acousticalsociety.org/content/terms. Download to IP: 128.187.97.22 On: Mon, 17 Mar 2014 20:38:46

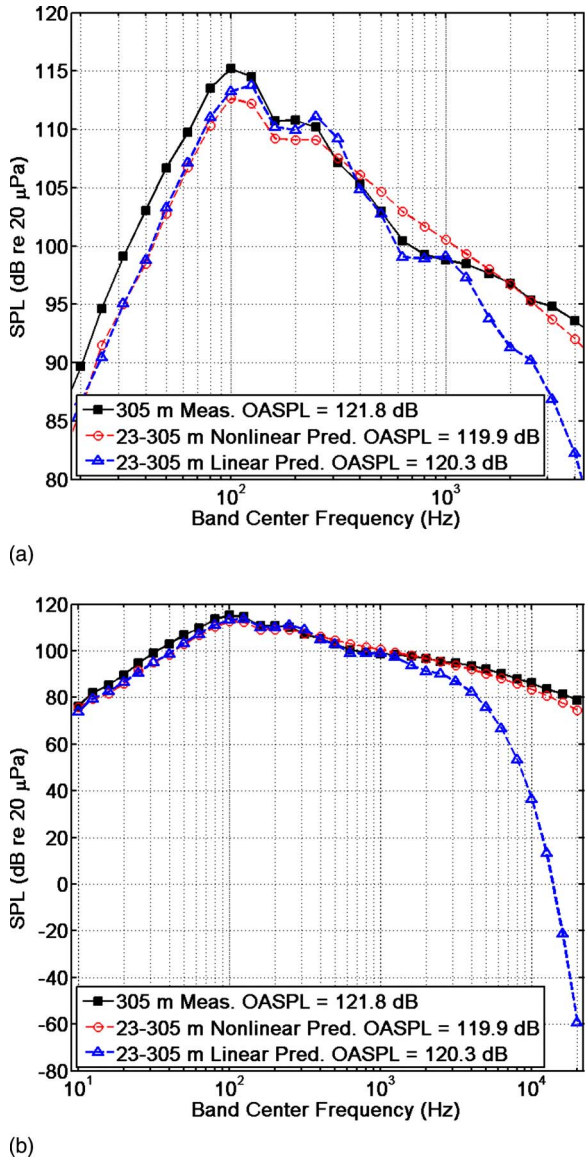

FIG. 8. (Color online) Comparison between predicted spectra and measurement for afterburner along 125°. In (a), the axes have been restricted to the same ranges used in the idle comparison (see Fig. 7). In (b), an expanded scale is shown, which shows the level of disagreement between the linear prediction and the measurement at high frequencies.

2. Afterburner

The afterburner run-up measurement whose results were discussed previously in Sec. IV A 3 was taken less than 1 min after the idle measurement. The results of the comparison between the predicted and measured spectra are displayed in Fig. 8(a), over the same limited frequency range as the idle comparison and also with a 40 dB vertical axis. A comparison between Figs. 8(a) and 7 reveals a similar low-frequency discrepancy between the model and measurement. Because the change in meteorological conditions during the course of the measurements was gradual, and the fact that this same discrepancy occurs in the low-amplitude idle measurement taken less than 1 min previously, it is believed that this low-frequency increase in spectral level relative to predictions is a linear, as opposed to a nonlinear, phenomenon.[29]

In contrast to the idle results from Fig. 7, the greatest disparity between the linear model and measurement for afterburner does not occur at low frequencies but rather above 2 kHz. In Fig. 8(a), the nonlinear prediction and measurement agree within 2 dB over this range, whereas there is a 12 dB difference between the linear prediction and the measurement. Extrapolating the spectral trends out to higher frequencies indicates that the difference between measurement and linear prediction should be much greater at the full analysis bandwidth of 20 kHz. This hypothesis is confirmed in Fig. 8(b), where the same afterburner prediction is shown on an expanded scale, from 10 Hz to 20 kHz. The difference between the measured spectrum and the nonlinear prediction is only about 4 dB for the 20 kHz one-third octave band, whereas the difference between the linear prediction and measured spectrum is 140 dB. Therefore, Fig. 8(b) represents strong evidence of how highly nonlinear the propagation of noise from a high-power jet can be.

The emphasis in these comparisons between predictions and measurement is on the one-third octave spectra because they conveniently demonstrate the average agreement between the predicted and measured noise waveforms and permit observation of behavior not readily seen in the time waveforms. However, because the models do, in fact, provide predicted waveforms and these waveforms are time aligned with the measured waveforms at 305 m, direct comparison of the predicted and measured waveforms is possible. The afterburner case has been chosen because the differences between the nonlinear and linear propagation predictions are easily seen. The nonlinearly and linearly predicted waveform segments at afterburner and for the same time segment as displayed in Fig. 5(b) are displayed in Fig. 9. The similarities between the waveform steepening in the nonlinear prediction from 23 m and the measured waveform are easily noted. On the other hand, the linear prediction at 305 m is only slightly smoother than the 23 m waveform in

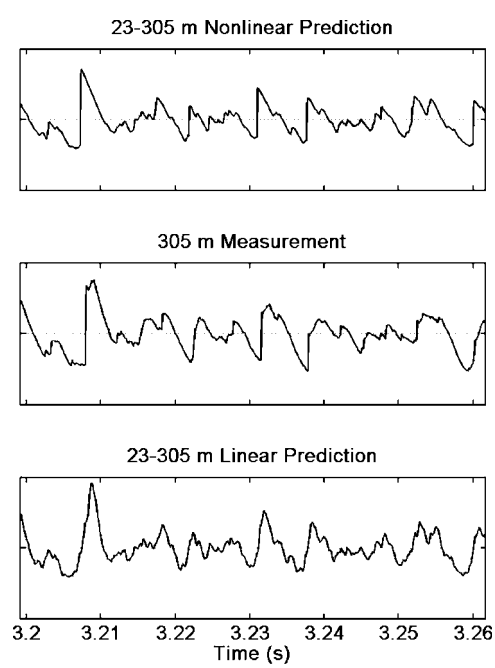

FIG. 9. Nonlinearly predicted, measured, and linearly predicted waveforms at 305 m. The ordinate limits for each waveform are ±140 Pa.

Redistribution subject to ASA license or copyright; see http://acousticalsociety.org/content/terms. Download to IP: 128.187.97.22 On: Mon, 17 Mar 2014 20:38:46

Fig. 5(b), which is due to the relatively low atmospheric absorption coefficient in the characteristic-frequency region and the inability to see the absorption-induced roll-off of the high-frequency content on this time scale.

3. 90% rpm

The previous results for afterburner showed that the propagation can be highly nonlinear, but what about other engine conditions where less thrust is provided? An intermediate engine condition is well represented by 90% rpm, which means that the turbomachinery in the engine is running at 90% of the rate of what it would be at military power (also commonly referred to as "Mil" power), which is 100% rpm. (Note that the afterburner yields both greater thrust and noise levels than military power.) Analysis of the measured one-third octave spectra, coupled with examination of the waveforms themselves, provided evidence that the propagation was, in fact, nonlinear. A comparison between the two models and the measured spectrum along 125° confirms this, first for the restricted range used in the comparison for idle and, second, for the expanded range, 10 Hz–20 kHz. These two comparisons are displayed in Figs. 10(a) and 10(b). The agreement between measurement and models at low frequencies is significantly better for this case than for the idle and afterburner comparisons, for which the data were taken about 10 min earlier. In Fig. 10(a), the disagreement between the measurement and linear model is only 7 dB at 4 kHz, less than it was for the afterburner case. However, with the expanded scale in Fig. 10(b), the disagreement between the measurement and linear prediction grows to more than 120 dB at 20 kHz, whereas there is only a 7 dB difference between the nonlinear model and the measurement. This again shows that the propagation along the peak radiation angle can be highly nonlinear, even for an intermediate-thrust engine setting. In other words, this result begins to establish the possible commonness of nonlinear propagation effects in noise radiated from a high-thrust military aircraft.

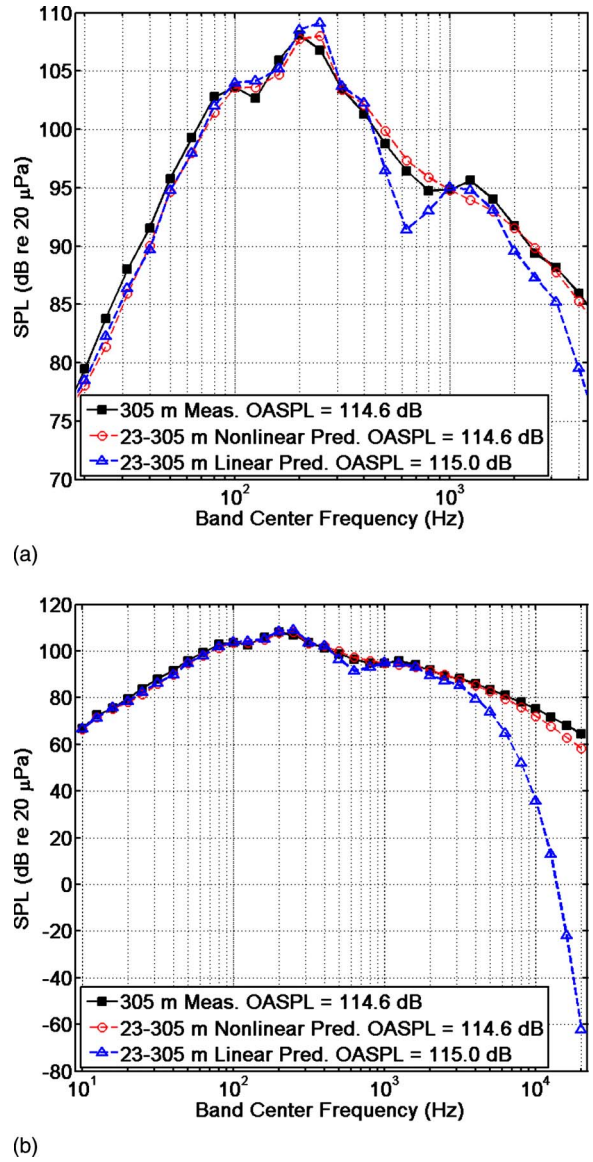

FIG. 10. (Color online) Comparison between predicted spectra and measurement for 90% rpm along 125°. In (a), the axes have been restricted to the same ranges used in the idle comparison (see Fig. 7). In (b), an expanded scale is shown.

B. Function of algorithm input distance

Before proceeding to a discussion of nonlinear propagation as a function of angle, it is first important to consider the issue of the algorithm input distance. The previously discussed comparisons for afterburner and 90% rpm showed good agreement between the nonlinear prediction and measurement, especially relative to the linear prediction. However, that agreement was only for one starting distance and it is possible that input waveforms acquired at different distances could yield different results, especially since it is likely that a microphone located at 23 m is not yet in the true geometric far field of the jet. To show the consistency of the propagation model results as a function of starting distance, the 125° afterburner and 90% rpm waveform data at 23, 61, and 152 m have been propagated with the GBE-based model out to 305 m. Their resulting one-third octave spectra are compared against the measured spectrum for the two engine settings in Fig. 11. The afterburner comparison in Fig. 11(a) reveals that the maximum difference between predicted spectra at any frequency is only about 1 dB. For the 90% rpm comparison in Fig. 11(b), the spread between nonlinearly predicted spectra is greater in that the 61–305 m predicted levels are too great above 400 Hz and the other prediction levels are too low above about 3 kHz. However, these results bound the measured spectrum at 305 m and represent relatively little error when compared to the spectra obtained with the linear model.

C. Function of angle

At this point, it has been established that nonlinearity affects the propagation along the peak radiation angle (125°) for intermediate- and maximum-thrust engine conditions. Furthermore, it has been verified that the results are relatively insensitive to the algorithm input distance. The remaining question to consider, therefore, is whether nonlinear propagation occurs only at the peak directivity angle or if it

Redistribution subject to ASA license or copyright; see http://acousticalsociety.org/content/terms. Download to IP: 128.187.97.22 On: Mon, 17 Mar 2014 20:38:46

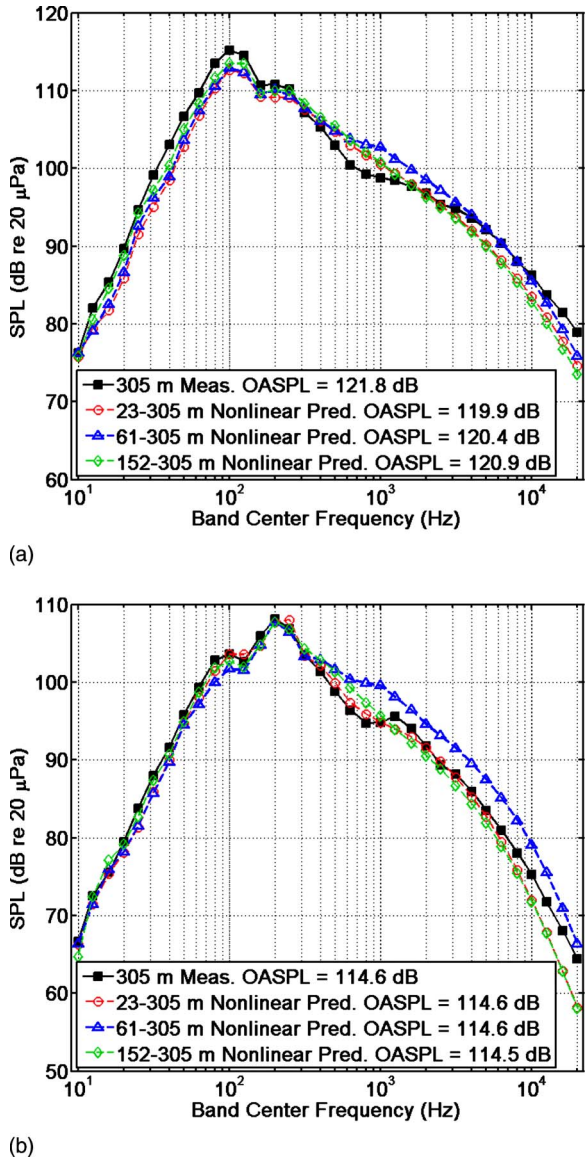

FIG. 11. (Color online) Comparison of various nonlinear predictions vs measurement along 125° as a function of algorithm starting distance for (a) afterburner and (b) 90% rpm.

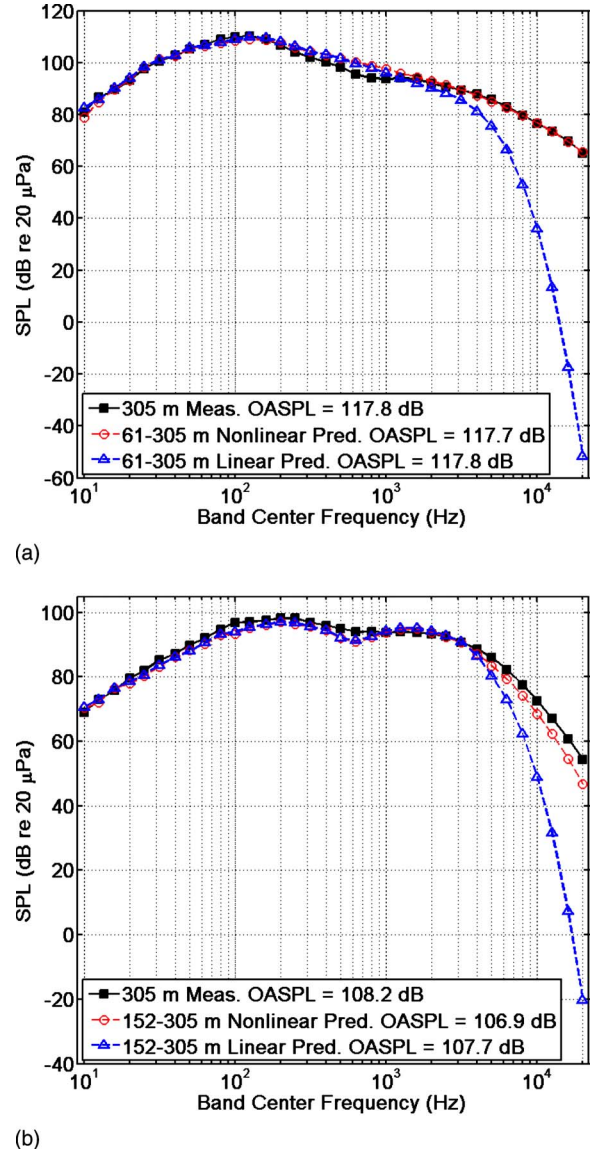

FIG. 12. (Color online) Comparisons between predicted spectra and measurement for afterburner along (a) 145° and (b) 90°.

is common at other angles as well. Because 145° and 90° represent the farthest angles from 125° over which predictions can be made, comparisons for these two angles are shown for both engine conditions.

Comparisons along 145° and 90° are shown for afterburner in Fig. 12 and for 90% rpm in Fig. 13. Figure 12(a) confirms what might have been supposed from an examination of the measured spectra as a function of angle in Fig. 6, that the nonlinearity present in the propagation along 145° is similar to that experienced along 125°. This is also true for the 90% rpm comparison in Fig. 13(a). However, the results along 90° are especially significant in that, although the afterburner case exhibits greater nonlinear effects [see Fig. 12(b)], the noise propagation at 90% rpm and 90° is also nonlinear, as demonstrated by the agreement between the nonlinear model and the measurement at high frequencies in Fig. 13(b). Note that the leveling off in the measured spectrum in Fig. 13(b) at 20 kHz is caused by the measurement system noise floor being reached somewhere in that one-third octave band. The fact that the propagation appears to be appreciably nonlinear at 90° could be considered surprising in that a bispectral analysis of afterburner measurements made on the F/A-18E Super Hornet[3] revealed no evidence of nonlinearity at that angle despite the fact that the F/A-18E's OASPL at close range was several decibels greater than that of the F-22A.

VI. CONCLUDING DISCUSSION

The results of the numerous comparisons between linear and nonlinear propagation models and measurements of the F-22A Raptor have resulted in several findings. First, it has been shown that the propagation can be significantly nonlinear, even at an intermediate-thrust engine setting (90% rpm). Second, these nonlinear effects, including 90% rpm, are not limited to the peak radiation angle but extend at least over the measurement aperture of 90°–145°. Third, despite the fact that the generalized-Burgers-equation-based model does

Redistribution subject to ASA license or copyright; see http://acousticalsociety.org/content/terms. Download to IP: 128.187.97.22 On: Mon, 17 Mar 2014 20:38:46

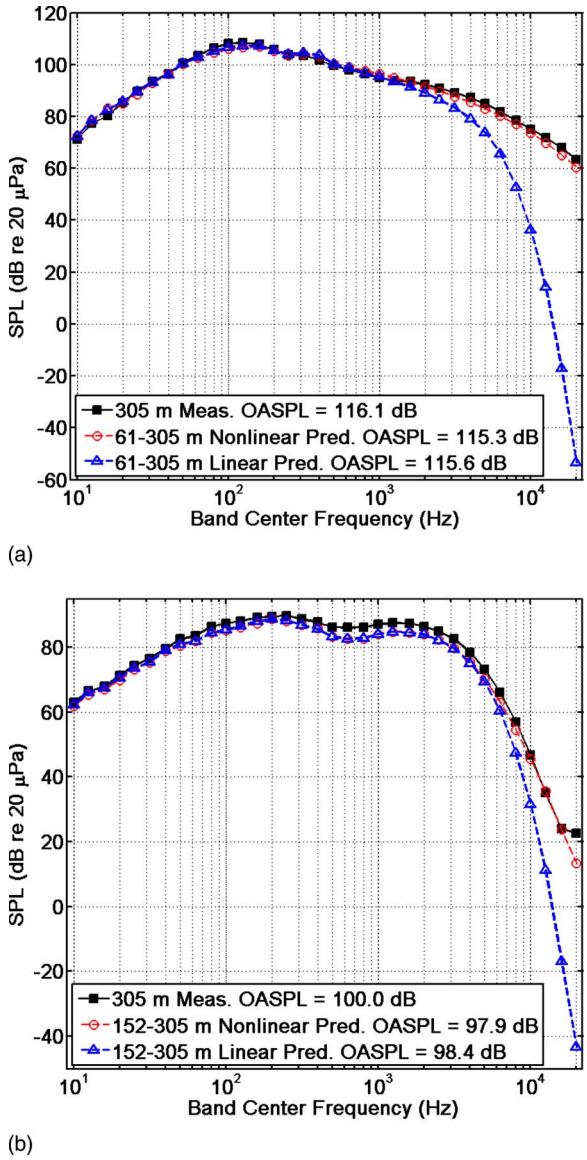

FIG. 13. (Color online) Comparisons between predicted spectra and measurement for 90% rpm along (a) 145° and (b) 90°.

not contain all the phenomena encountered in the actual measurement (i.e., a variable atmosphere and multipath interference), favorable agreement between the measurement and the nonlinear model has been obtained for all cases considered, especially relative to the linear propagation model. These findings illustrate the likely prevalence of nonlinear propagation effects in the noise radiated by high-power jet aircraft, a question that has been debated for more than 30 years.

Although there is more to be done in terms of model refinement (e.g., the inclusion of multipath effects caused by the ground or turbulence), a potentially important direction for future research efforts is to investigate the impact of these nonlinear propagation effects on communities and individuals. From a community noise standpoint, one could study the results presented in this article and potentially conclude that, although significant nonlinear effects occur in the propagation, the impact of nonlinearity on the predicted OASPL is minimal, less than the experimental uncertainty associated with typical outdoor measurements. If this line of reasoning is coupled with recent findings[30] showing that nonlinear propagation of a waveform with a jet-noise-like spectrum may not significantly affect common single-number metrics, such as A-weighted OASPL, perceived noise level, Stevens Mark-VII loudness, and Zwicker loudness, it could result in a conclusion that nonlinear effects, though scientifically interesting, are unimportant to human perception.

However, we believe that, based on the conclusions of Ref. 30, the potential significance of nonlinear propagation effects related to human perception merits further investigation. Although Ref. 30 demonstrates that nonlinear propagation causes little change in calculated single-number metrics, it also contains multimedia content that encourages the reader to listen to the results of nonlinear versus linear propagation. Even though the nonlinearly and linearly propagated waveforms have nearly equal overall levels, as determined with the several common metrics discussed previously, the nonlinear waveform is perceived to be dramatically different than the linear waveform upon playback. Given the likely prevalence of nonlinear effects in high-power jet noise propagation, this significant difference in noise perception caused by nonlinearity is a topic that needs to be fully addressed in future research.

ACKNOWLEDGMENTS

K. L. Gee, V. W. Sparrow, J. M. Downing, M. M. James, and C. M. Hobbs were supported by the Strategic Environmental Research and Development Program. T. B. Gabrielson and A. A. Atchley were supported by the Office of Naval Research. The authors are grateful to Dr. Sally Anne McInerny of the University of Alabama-Birmingham for useful discussions during the course of this research. Robert McKinley, John Hall, and Frank Mobley of the Air Force Research Laboratory are also acknowledged for their roles in the measurement portion of this investigation.

[1]C. L. Morfey and G. P. Howell, "Nonlinear propagation of aircraft noise in the atmosphere," AIAA J. **19**, 986–992 (1981).
[2]K. L. Gee, T. B. Gabrielson, A. A. Atchley, and V. W. Sparrow, "Preliminary analysis of nonlinearity in military jet aircraft noise propagation," AIAA J. **43**, 1398–1401 (2005).
[3]K. L. Gee, A. A. Atchley, L. E. Falco, T. B. Gabrielson, and V. W. Sparrow, "Bispectral analysis of high-amplitude jet noise," AIAA (2005), Paper No. AIAA-2005-2937.
[4]J. A. Gallagher and D. K. McLaughlin, "Experiments on the non-linear characteristics of noise propagation from low and moderate Reynolds number supersonic jets," AIAA (1981), Paper No. AIAA-81-2041.
[5]B. P. Petitjean, D. K. McLaughlin, and K. Viswanathan, "Acoustic pressure waveforms measured in high speed jet noise experiencing nonlinear propagation," AIAA (2005), Paper No. AIAA-2005-0209.
[6]K. L. Gee, M. R. Shepherd, L. E. Falco, A. A. Atchley, L. S. Ukeiley, B. J. Jansen, and J. M. Seiner, "Identification of nonlinear and near-field effects in jet noise using nonlinearity indicators," AIAA (2007), Paper No. AIAA-2007-3653.
[7]D. F. Pernet and R. C. Payne, "Non-linear propagation of signals in air," J. Sound Vib. **17**, 383–396 (1971).
[8]F. M. Pestorius and D. T. Blackstock, "Propagation of finite-amplitude noise," in *Finite-Amplitude Wave Effects in Fluids*, edited by L. Bjorno (IPC Science and Technology, Guildford, 1973), pp. 24–29.
[9]A. D. Pierce, "Progressive wave equations and algorithms for sonic boom propagation," *Proceedings of Noise-Con 93* (Noise Control Foundation, Poughkeepsie, NY, 1993), pp. 157–162.
[10]D. T. Blackstock, "Nonlinear propagation of jet noise," in *Proceedings of*

Redistribution subject to ASA license or copyright; see http://acousticalsociety.org/content/terms. Download to IP: 128.187.97.22 On: Mon, 17 Mar 2014 20:38:46

the third Interagency Symposium on University Research in Transportation Noise (University of Utah, Salt Lake, UT, 1975), pp. 389–397.
[11]D. A. Webster and D. T. Blackstock, "Experimental investigation of outdoor propagation of finite-amplitude noise," NASA Contractor Report 2992, Applied Research Laboratories, The University of Texas at Austin, Austin, TX, 1978.
[12]K. L. Gee, V. W. Sparrow, M. M. James, J. M. Downing, and C. M. Hobbs, "Measurement and prediction of nonlinearity in outdoor propagation of periodic signals," J. Acoust. Soc. Am. **120**, 2491–2499 (2006).
[13]D. G. Crighton and S. Bashforth, "Nonlinear propagation of broadband jet noise," AIAA (1980), Paper No. AIAA-80-1039.
[14]J. F. Scott, "The nonlinear propagation of acoustic noise," Proc. R. Soc. London, Ser. A **383**, 55–70 (1982).
[15]J. Lighthill, "Some aspects of the aeroacoustics of high speed jets," NASA Contractor Report 191458, ICASE Report No. 93-20, 1993.
[16]J. N. Punekar, "Numerical simulation of nonlinear random noise," Ph.D. thesis, University of Southampton, Southampton, UK, 1996.
[17]P. Menounou and D. T. Blackstock, "A new method to predict the evolution of the power spectral density for a finite-amplitude sound wave," J. Acoust. Soc. Am. **115**, 567–580 (2004).
[18]K. L. Gee, "Prediction of nonlinear jet noise propagation," Ph.D. thesis, The Pennsylvania State University, University Park, PA, 2005.
[19]M. O. Anderson, "The propagation of a spherical N wave in an absorbing medium and its diffraction by a circular aperture," Technical Report No. ARL-TR-74-25, Applied Research Laboratories, The University of Texas at Austin, Austin, TX, 1974.
[20]K. L. Gee and V. W. Sparrow, "Quantifying nonlinearity in the propagation of noise from military jet aircraft," in *CD-ROM: Proceedings of Noise-Con 05*, edited by J. S. Bolton, P. Davies, and G. C. Maling, Jr. (Institute of Noise Control Engineering of the USA, Washington, DC, 2005), Paper No. nc05_194.
[21]K. L. Gee, V. W. Sparrow, M. M. James, J. M. Downing, C. M. Hobbs, T. B. Gabrielson, and A. A. Atchley, "Measurement and prediction of noise propagation from a high-power jet aircraft," AIAA J. **45**, 3003–3006 (2007).
[22]L. C. Sutherland and G. A. Daigle, "Atmospheric sound propagation," in *Encyclopedia of Acoustics*, edited by M. J. Crocker (Wiley, New York, 1997), Chap. 32, pp. 341–365.
[23]K. Attenborough, S. I. Hayek, and J. M. Lawther, "Propagation of sound above a porous half-space," J. Acoust. Soc. Am. **68**, 1493–1501 (1980).
[24]G. A. Daigle, "Effects of atmospheric turbulence on the interference of sound waves above a finite impedance boundary," J. Acoust. Soc. Am. **65**, 45–49 (1979).
[25]S. N. Gurbatov and O. V. Rudenko, "Statistical phenomena," in *Nonlinear Acoustics*, edited by M. F. Hamilton and D. T. Blackstock (Academic, San Diego, 1998), Chap. 13, pp. 377–398.
[26]These linear predictions differ slightly from those presented in Refs. 18, 20, and 21, which used a one-third octave band spectrum as input and simply applied the absorption coefficient for each of the band center frequencies. However, this can lead to erroneous predictions of atmospheric absorption losses in those bands where the energy is primarily distributed at one of the band edges. See Refs. 27 and 28 for relevant discussion.
[27]L. C. Sutherland andH. E. Bass, "Influence of atmospheric absorption on the propagation of bands of noise," J. Acoust. Soc. Am. **66**, 885–894 (1979).
[28]G. P. Howell and C. L. Morfey, "Finite bandwidth corrections applicable to noise spectra shaped by atmospheric attenuation," J. Acoust. Soc. Am. **72**, 1574–1582 (1982).
[29]The differences between the predictions and measurement for the idle case were used in Ref. 21 to empirically correct the predictions made for the afterburner case, which greatly improved the predictions over that frequency range.
[30]K. L. Gee, S. H. Swift, V. W. Sparrow, K. J. Plotkin, and J. M. Downing, "On the potential limitations of conventional sound metrics in quantifying perception of nonlinearly propagated noise," J. Acoust. Soc. Am. **121**, EL1–EL7 (2007).

Redistribution subject to ASA license or copyright; see http://acousticalsociety.org/content/terms. Download to IP: 128.187.97.22 On: Mon, 17 Mar 2014 20:38:46